Catalysis Today 145 (2009) 258–266

Contents lists available at ScienceDirect

Catalysis Today

journal homepage: www.elsevier.com/locate/cattod

Solid-state kinetics and catalytic behavior of selective oxidation catalysts from time-resolved XAFS investigations

T. Ressler *

Technische Universität Berlin, Institut für Chemie, Sekr. C2, Strasse des 17, Juni 135, D-10623 Berlin, Germany

ARTICLE INFO

Article history:
Available online 21 March 2009

Keywords:
In situ
Time-resolved
Heterogeneous catalysis
Structure–activity relationships
EXAFS spectroscopy
X-ray absorption
Molybdenum
Oxides
Selective oxidation
Reduction
Oxidation
Solid-state kinetics

ABSTRACT

Time-resolved measurements are required to elucidate time-dependencies of the electronic and geometric structure of a catalyst under changing reaction conditions. Monitoring the evolution of the bulk structure of a catalyst under changing conditions reveals the solid-state kinetics of the corresponding reaction. X-ray absorption spectroscopy (XAS) permits to reveal quantitative phase composition and average valence together with the evolution of the local structure. Hence, combining time-resolved XAS with simultaneous catalysis measurements may elucidate correlations between catalytic performance, the catalyst state under reaction conditions, and its solid-state kinetics. Here, results from time-resolved in situ XAS investigations of various molybdenum-based selective oxidation catalysts are compared and discussed. Model systems (i.e. α-MoO_3, hexagonal MoO_3 supported on SBA-15, and $H_4[PVMo_{11}O_{40}]$) suitable to distinguish structural effects and promotion by additional metal centers have been studied under changing reaction conditions. Correlations between reduction and oxidation solid-state kinetics and catalytic performance reveal the dependence of the selectivity of the catalyst on its electronic structure. In particular the re-oxidation kinetics and the average valence under reaction conditions appear to be determined by the defect structure of the underlying catalyst bulk.

1. Introduction

Molybdenum oxide based catalysts are extensively employed for selective oxidation of alkanes or alkenes [1–4]. Selective oxidation of alkenes with gas phase oxygen is commonly believed to proceed via a reduction-oxidation (“redox”) mechanism (Mars-van-Krevelen mechanism) [5–7]. It consists of alternating oxidation and reduction of the metal oxide catalyst surface and/or bulk. Selective oxidation of propene, for instance, starts with adsorption of propene on the surface of the catalyst, abstraction of hydrogen, and the formation of an allylic species [8,9]. Subsequently, oxygen from the bulk of the catalyst may be incorporated in the allylic species affording the selective oxidation product acrolein or the total oxidation product carbon dioxide. Eventually, the remaining oxygen vacancies on the surface or in the bulk of the catalyst are refilled by oxygen from the gas phase.

Depending on the redox potential of the gas phase, the electronic and geometric structure of molybdenum oxides changes under reaction conditions. According to the redox mechanism the resulting (defect) bulk and surface structure is determined by the oxidation and reduction kinetics of the catalyst bulk. The time-averaged state of a molybdenum-based catalyst under reaction conditions may appear invariant. However, the nature of this state is governed by its dynamic behavior as a function of the redox potential of the gas phase. Incomplete re-oxidation, for instance, will result in a partially reduced catalyst, whereas fast oxidation and slow reduction will result in high average oxidation state under reaction conditions. Achieving a comprehensive understanding of structure–activity correlations is unthinkable without knowledge on the time-dependencies of electronic and geometric structure on changing gas phase redox potential.

In situ studies on heterogeneous catalysts are indispensable in modern catalysis research (refer to recent monographs [10] for further reading). Reliable correlations between the structure of a catalyst and its catalytic performance can only be determined under relevant reaction conditions. These structure activity correlations constitute the foundation of a knowledge-based design of novel heterogeneous catalysts [11]. However, investigating a solid heterogeneous catalyst under steady-state reaction conditions yields little information on the dynamic nature of its surface and bulk structure. Therefore, time-resolved measurements are required to further elucidate the behavior of the

* Tel.: +49 30 314 79736; fax: +49 30 314 21106.
E-mail address: thorsten.ressler@tu-berlin.de.

0920-5861/$ – see front matter © 2009 Elsevier B.V. All rights reserved.
doi:10.1016/j.cattod.2009.02.011

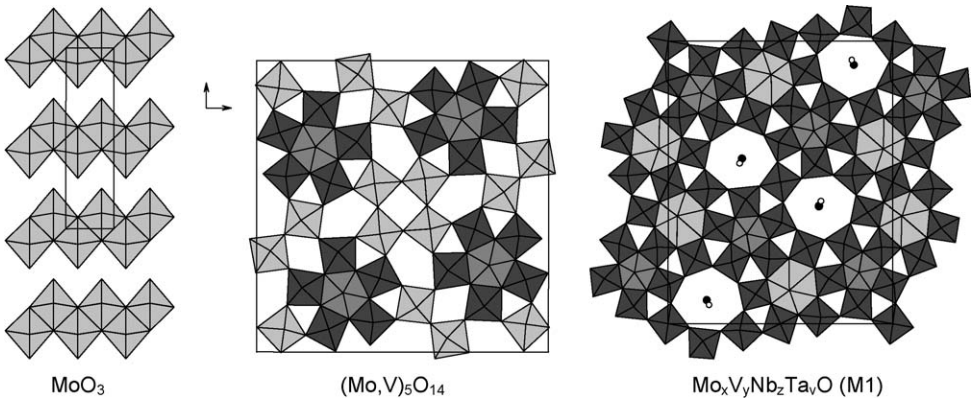

Fig. 1. Schematic representation of the increasing structural and compositional complexity of various molybdenum oxide based selective oxidation catalyst.

electronic and geometric structure of a catalyst under changing reaction conditions. Monitoring the gas phase composition during a catalytic reaction yields conventional kinetic information. Conversely, monitoring bulk structural changes reveals the solid-state kinetics of dynamic structural changes in the bulk of the catalyst under reaction conditions. Hence, only combining time-resolved XAS with simultaneous rapid activity measurements permits to obtain correlations between catalytic performance and the kinetics of bulk structural changes.

Both binary molybdenum oxide (Mo_xO_y) and mixed Mo oxides exhibit a rich structural chemistry. Various modification exist possessing different average oxidation states (e.g. Magnelli phases, Mo_xO_{3n-1} ($x = 8, 9$)) and different structures without (e.g. orthorhombic α-MoO_3 and hexagonal MoO_3) or with additional metal centers (e.g. (Mo, V, W)$_5O_{14}$, $Mo_xV_yNb_zTa_vO$ (M1 phase)). In particular the latter have been found to exhibit superior catalytic activity and selectivity. However, with respect to structure–activity correlations it is intrinsically difficult to distinguish between structural and compositional effects. This is mostly because bulk structure and composition are modified simultaneously resulting in an undesired increase in complexity (Fig. 1). Hence, suitable model systems are required that permit altering the structure without changing the chemical composition and vice versa. Thereby, the beneficial effect of additional metal centers and particular structural motifs can be disentangled.

In the following, three suitable model systems for molybdenum-based selective oxidation catalysts are briefly introduced. First, orthorhombic molybdenum trioxide, α-MoO_3, constitutes the archetype of an active binary model catalyst for the oxidation of propene [1]. Second, heteropolyoxomolybdates (HPOM) of the Keggin type (e.g. $H_3[PMo_{12}O_{40}]$) are model catalysts for the partial oxidation of alkanes and alkenes [12,13]. HPOM are capable of accommodating additional metal centers while retaining their particular molecular structure. Third, supported molybdenum oxides can be chosen to investigate binary molybdenum oxides other than α-MoO_3 under relevant reaction conditions. Interaction with the support stabilizes particular structures which would otherwise decompose into the more stable bulk α-MoO_3. In the present work, the results of time-resolved XAS investigations of the molybdenum oxide model systems described above are being compared and discussed. Time-dependent changes in average oxidation state are correlated with the catalytic performance of the materials studied. A comparison of the results obtained is meant to emphasize both the capabilities of time-resolved XAFS studies and the correlation between reduction–oxidation kinetics, average Mo valence, and catalytic performance of the various Mo oxides investigated.

2. Experimental

2.1. Sample preparation and characterization

Molybdenum trioxide (MoO_3) was prepared by thermal decomposition of ammonium heptamolybdate (AHM), $(NH_4)_6Mo_7O_{24}\cdot 4H_2O$ (*Aldrich Co.*), in flowing synthetic air (RT – 773 K with 2 K/min, held for 2 h at 773 K). Phase purity of the compound obtained was verified by XRD. Characterization details can be found in Ref. [14,15]. Preparation of heteropolyoxomolybdates was conducted according to previously described procedures [16,17]. Depending on the composition of the V containing HPOM MoO_3 and V_2O_5 were suspended in water. The corresponding amount of phosphoric acid (H_3PO_4) was added dropwise to the boiling and stirred suspension of the metal oxides. After complete addition of the phosphoric acid a clear amber colored solution was obtained. The solid product was isolated by removing the solvent in a rotary evaporator at ~363 K and dried in a vacuum desiccator. Thermal analysis studies (TG/DTA-MS) confirmed a similar thermal stability of as-prepared $H_5[PV_2Mo_{10}O_{40}]\cdot 13H_2O$ and $H_4[PVMo_{11}O_{40}]\cdot 13H_2O$.

SBA-15 used as a support for MoO_3 was prepared according to literature procedures [32]. 1 g of SBA-15 was stirred in aqueous solutions containing ammonium heptamolybdate (0.09 mol/L) at pH 7–8 and room temperature for 18 h. The impregnated SBA-15 was calcined at 773 K for 3 h in air to obtain MoO_3. The Mo loading of the catalysts was 13 wt.% and the synthesized products were stored in dried air. Further details on the preparation procedure and structural characterization of the material obtained are provided in Ref. [18]. Phase purity and structure of the reference oxides (hex-MoO_3, ICSD 75417) were confirmed by X-ray powder diffraction.

2.2. X-ray absorption spectroscopy (XAS)

In situ transmission XAS experiments were performed at the Mo K edge (19.999 keV) at beamline X1 at the *Hamburg Synchrotron Radiation Laboratory*, HASYLAB, using a Si(3 1 1) double crystal monochromator (measuring time ~4 min/scan) (energy dispersive XAS data were obtained at beamline ID 24 at ESRF, Grenoble. Details are provided in the cited literature). The storage ring operated at 4.4 GeV with injection currents of 150 mA. The in situ experiments were conducted in a flow-reactor at atmospheric pressure in flowing reactants (total flow ~30 ml/min, available temperature range from 300 K to 773 K, heating rate 4 K/min). The gas phase composition at the cell outlet was continuously monitored using a non-calibrated mass spectrometer in a multiple ion detection mode (QMS200 from *Pfeiffer*). Conversion of propene was estimated from the propene ion

current (m/e 42) before and during reaction to be about 10% at 723 K. The various molybdenum oxides were mixed with boron nitride (~7 mg MoO_x, ~30 mg BN) and pressed with a force of 1 ton into a 5 mm in diameter pellet resulting in an edge jump at the Mo K edge of $\Delta\mu_x \sim 1$. Supported hex-MoO_3-SBA-15 was employed as-is. X-ray absorption fine structure (XAFS) analysis was performed using the software package WinXAS 3.1 [19] Background subtraction and normalization were carried out by fitting linear polynomials to the pre-edge and the post-edge region of an absorption spectrum, respectively. The extended X-ray absorption fine structure (EXAFS) $\chi(k)$ was extracted by using cubic splines to obtain a smooth atomic background, $\mu_0(k)$. The radial distribution function FT($\chi(k)$) was calculated by Fourier transforming the k^3-weighted experimental $\chi(k)$ function, multiplied by a Bessel window, into the R space. EXAFS data analysis was performed using theoretical backscattering phases and amplitudes calculated with the ab-initio multiple-scattering code FEFF7 [20]. Single-scattering and multiple-scattering paths in the corresponding model structures were calculated up to 6.0 Å with a lower limit of 4.0% in amplitude with respect to the strongest backscattering path. EXAFS refinements were performed in R space simultaneously to magnitude and imaginary part of a Fourier transformed k^3-weighted and k^1-weighted experimental $\chi(k)$ using the standard EXAFS formula (k range from 3.4 to 15.1 $Å^{-1}$, R range 0.7–4.1 Å) [21]. Structural parameters determined are (i) one E0 shift, (ii) Debye–Waller factors for single-scattering paths, and (iii) distances of single-scattering paths. Coordination numbers (CN) and S_0^2 were kept invariant in the refinement.

3. Results and discussion

3.1. Solid-state kinetics of reduction and re-oxidation of α-MoO_3

α-MoO_3 oxidizes propene in the presence of oxygen at temperatures above ~600 K [1]. Under reaction conditions, MoO_3 exhibits a slightly reduced average valence, which, according to the conventional redox mechanism, can be attributed to different rates for reduction and re-oxidation of molybdenum trioxide [22–25]. Reduction of MoO_3 in propene and oxidation of MoO_2 in oxygen were investigated by time-resolved XAFS combined with mass spectrometry [14,26]. The evolution of Mo K edge spectra of MoO_3 and the different kinetics of the reduction and the re-oxidation are displayed in Fig. 2. Apparently, MoO_3 is completely and rapidly reduced to MoO_2. Subsequently, at elevated temperatures MoO_2 is even faster re-oxidized to MoO_3.

As an example for the analysis of the solid-state kinetics, Fig. 3 shows the extent of reduction (α) during isothermal reduction of MoO_3 in 5 vol.% propene at 723 K, 10 vol.% propene at 673 K, and 10 vol.% propene at 698 K. The acceleratory regime of the reduction at 673 K (up to $\alpha \approx 0.3$) can be described by a power rate law ($\alpha \sim t^2$), whereas the deceleratory regime of the reduction can be described by a "three dimensional diffusion" rate law ($\alpha \sim 1 - (1 - t^{1/2})^3$). Moreover, the solid-state kinetics of the reduction of MoO_3 in propene exhibits a change in the rate-limiting step both as a function of temperature and as a function of the extent of reduction α. With increasing α at a given temperature, transition from a nuclei growth kinetics to a three dimensional diffusion controlled regime is observed. With decreasing temperature (<~650 K) a pronounced transition from a nuclei growth kinetics to a regime that is entirely controlled by oxygen diffusion in the MoO_3 lattice was found. Hence, a schematic reaction mechanism for the reduction of MoO_3 in propene consists of (i) generation of oxygen vacancies at the (1 0 0) or (0 0 1) facets by reaction with propene, (ii) vacancy diffusion in the MoO_3 bulk, (iii) formation of "$Mo_{18}O_{52}$" type shear-structures in the lattice, and (iv) formation and growth of MoO_2 nuclei. The re-oxidation of

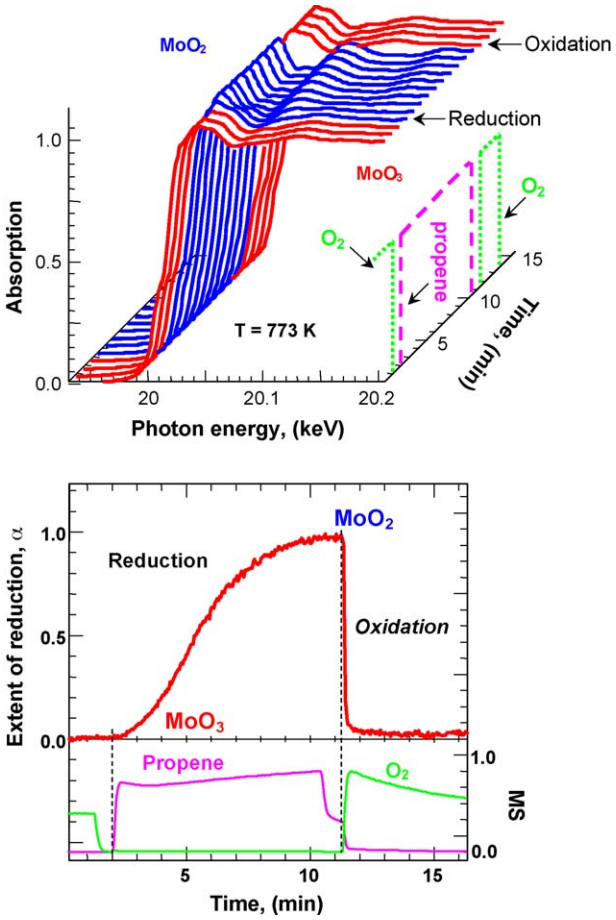

Fig. 2. Evolution of Mo K near-edge spectra of MoO_3 during isothermal switching of the gas phase from oxidizing conditions (oxygen) to reducing conditions (propene) (top). The extent of reduction α reflects the different kinetics of the reduction and re-oxidation of MoO_3 at 773 K (bottom).

MoO_2 in oxygen basically proceeds from step (iv) through (i). Complete re-oxidation to MoO_3, though, is obtained only at temperatures above 720 K [14].

In addition to studying the reduction and oxidation properties of MoO_3, the evolution of characteristic defects in the bulk structure of MoO_3 was investigated by time-resolved in situ XAS under propene oxidation conditions (273 K to 773 K, and propene to oxygen ratio from 1:1 to 1:5 [27]). The onset temperature of the reaction of propene and oxygen in the presence of MoO_3 coincides with the onset of the reduction of MoO_3 (~620 K) (Fig. 4). At temperatures below ~720 K and independent of the atmosphere used, partial reduction of MoO_3 is observed resulting in the formation of "$Mo_{18}O_{52}$" type defects in the layer structure of α-MoO_3 (Fig. 5). At temperatures above ~720 K and in oxygen or in a strongly oxidizing atmosphere, the "$Mo_{18}O_{52}$" type defects are re-oxidized to MoO_3 (increasing average valence in Fig. 5).

Combining the interpretation of the solid-state kinetics of reduction and re-oxidation of MoO_{3-x}, three stages of the structural evolution of MoO_{3-x} under selective oxidation conditions are distinguished (Fig. 6). (i) At temperatures below ~600 K selective oxidation of propene and participation of oxygen from the MoO_3 bulk are negligible. (ii) At temperatures between ~600 K and ~700 K oxygen vacancy diffusion in the bulk is sufficient to make a redox mechanism feasible. Because complete re-oxidation of the "$Mo_{18}O_{52}$" type shear-structures is inhibited, a partially reduced MoO_3 with crystallographic-shear (CS) lattice planes is obtained under reaction conditions. (iii) At temperatures above ~700 K sufficiently fast oxygen diffusion in the lattice combined

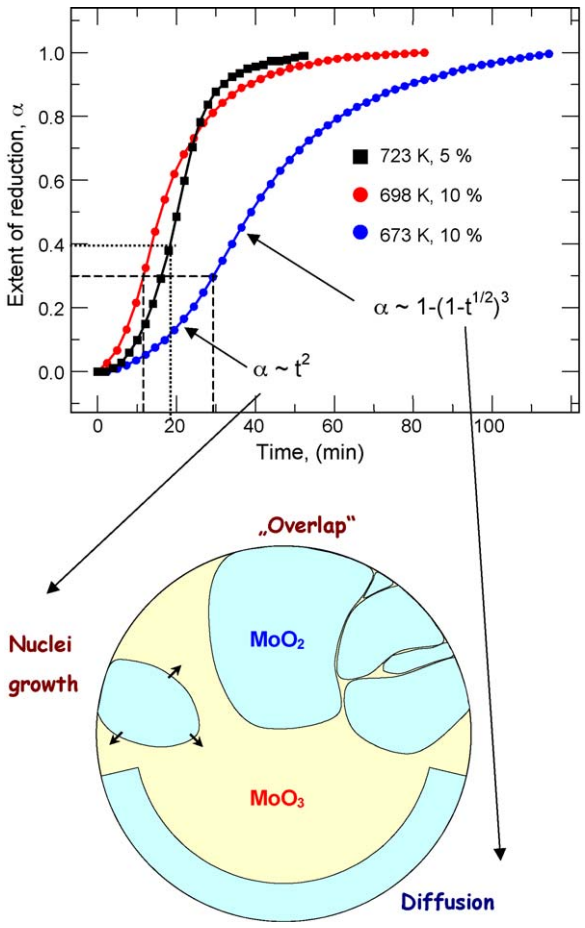

Fig. 3. Extent of reduction α obtained from in situ XAFS experiments during isothermal reduction of MoO_3 in 5 vol.% propene at 723 K, in 10 vol.% propene at 673 K, and in 10 vol.% propene at 698 K. The changes in the rate-limiting step from an $\alpha \sim t^2$ rate law (power law) to an $\alpha \sim 1 - (1 - t^{1/2})^3$ rate law (three dimensional diffusion) for the experiments at 673 K in 5 vol.% ($\alpha \approx 0.30$) and at 723 K in 10 vol.% ($\alpha \approx 0.4$) are indicated by a dashed and a dotted line, respectively.

with rapid formation and annihilation of CS permits the participation of a considerable amount of the lattice oxygen of MoO_3 in the partial oxidation of propene. The reduced average Mo valence of MoO_{3-x} under reaction conditions at temperature below ~700 K correlates with the inferior selectivity of the material [28]. Increasing reaction temperature and oxidation potential of the gas phase results in complete re-oxidation to MoO_3. While quantitative catalysis measurements are currently lacking, the increased average Mo valence appears to be correlated with an improved relative selectivity of the material under propene oxidation conditions [27].

3.2. Correlation between average valence and catalytic selectivity of heteropolyoxomolybdates

Because of their molecular structure, HPOM of the Keggin type (e.g. $H_3[PMo_{12}O_{40}]$) have been frequently employed as suitable model systems for more complex molybdenum-based mixed oxide catalysts. However, the "real structure" of the Keggin ion under reaction conditions is not necessarily identical to the ideal structure of the corresponding as-prepared heteropolyoxomolybdate. We have recently shown, that the onset of catalytic activity during thermal activation of $H_3[PMo_{12}O_{40}]\cdot 13\ H_2O$ and $H_4[PVMo_{11}O_{40}]\cdot 13\ H_2O$ in propene coincides with a partial decomposition of the Keggin ion at ~600 K and migration of Mo centers on extra-Keggin sites [29,30].

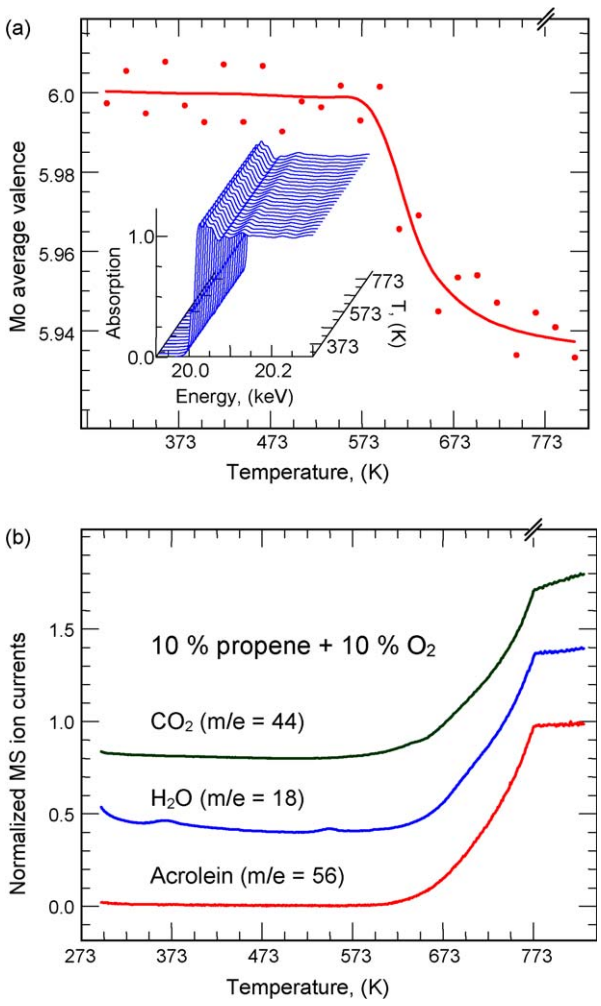

Fig. 4. (a) Evolution of Mo K edge position (relative to the edge position of MoO_3 and displaced for clarity) during temperature-programmed reaction of propene and oxygen in the presence of MoO_3 (10% O_2 and 10% propene in He) (300–773 K, 5 K/min, held at 773 K) (inset shows evolution of XANES spectra during TPR). (b) Evolution of the corresponding gas phase composition (CO_2 ($m/e = 44$), H_2O ($m/e = 18$), acrolein ($m/e = 56$)) during temperature-programmed reaction of propene and oxygen.

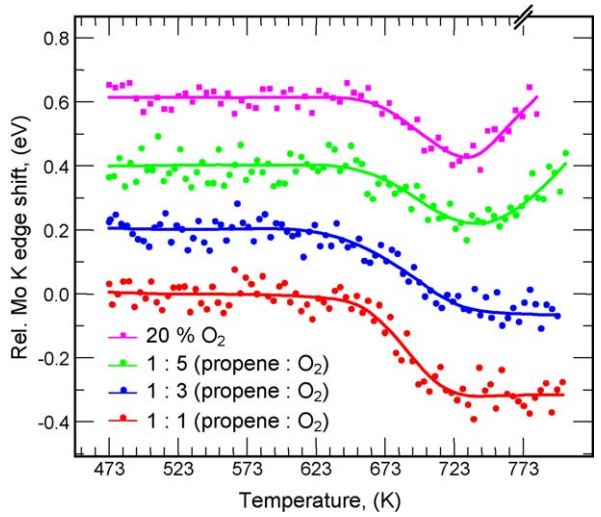

Fig. 5. Evolution of Mo K edge position (relative to the edge position of MoO_3 and displaced for clarity) during thermal treatment of MoO_3 in oxygen (20% in He) and during temperature-programmed reaction of propene and oxygen in the presence of MoO_3 (10% O_2 and 10% propene in He) (473–773 K, 10 K/min, held at 773 K). Three different ratios of oxygen and propene employed are indicated.

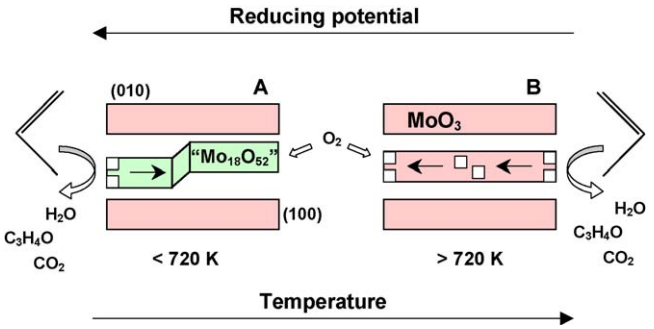

Fig. 6. Schematic representation of the structure of MoO_3 under reaction conditions (propene and oxygen) as a function of temperature and reduction potential of the gas phase. (A) Below 720 K or in a reducing gas phase. (B) Above 720 K and in an oxidizing gas phase. "$Mo_{18}O_{52}$" refers to crystallographic-shear type defects in the MoO_3 structure (squares indicate oxygen vacancies).

Time-resolved in situ XAS studies on activated $H_4[PVMo_{11}O_{40}]$ and $H_5[PV_2Mo_{10}O_{40}]$ oxidation catalyst were performed to obtain correlations between the dynamic structure and the catalytic selectivity of the material (time-resolution of ~30 s/spectrum [31]). Similar studies have been performed on vanadium free activated $H_3[PMo_{12}O_{40}]$ [29]. In the work discussed here, vanadium centers in the materials were additionally employed as probe of the local structure of the active site. Therefore, the local structure around the V centers in the catalyst under reaction conditions was elucidated by a detailed EXAFS analysis. Fig. 7 shows the experimental and theoretical FT($\chi(k)k^3$) and a schematic representation of the proposed active site thermally treated $H_4[PVMo_{11}O_{40}]$ catalysts. This example emphasizes the excellent capabilities of XAFS to elucidate both electronic and local geometric structure of metastable heterogeneous catalysts under relevant reaction conditions.

In addition to stationary in situ studies, the gas phase composition was isothermally switched from a reducing (propene) to an oxidizing (propene and oxygen) atmosphere (complete exchange in about 20 s in the in situ cell used) [31]. As an example, the evolution of the average Mo valence under reducing and oxidizing conditions at 698 K is depicted in Fig. 8. In contrast to α-MoO_3, HPOM were not fully reduced to MoO_2 during treatment in propene. However, under reducing conditions (propene) reaction temperatures above 673 K were accompanied by a slow but pronounced decrease of the average valence of the Mo centers in the activated catalyst (Fig. 8). The more reduced catalyst at 698 K exhibited a prolonged re-oxidation behavior (Fig. 8). The corresponding extent of re-oxidation curve could be simulated with a solid-state kinetic model assuming three-dimensional diffusion to be the rate-limiting step (Fig. 8).

Upon switching from propene and oxygen to propene at 673 K, the average Mo valence exhibited a reduction from 6 to 5.94. Apparently, at 673 K the reduction of the Mo centers in the lacunary Keggin ions is mostly limited to the surface of the accessible crystallites. This is again much in contrast to α-MoO_3. Upon switching to oxidizing conditions (propene and oxygen) at 673 K, the catalyst was rapidly re-oxidized. Intriguingly, the selectivity of the catalyst exhibited a pronounced correlation with the degree of reduction and the solid-state kinetics of the re-oxidation process. After the reductive treatment in propene and switching back to propene and oxygen at 673 K, the rapid re-oxidation of the catalyst was accompanied by a rapid increase in the concentration of both acrolein and CO_2 in the gas phase [31]. This indicates that the entirely re-oxidized catalyst quickly regains its activity and selectivity in propene oxidation. Conversely, with increasing reaction temperature (i.e. 698 K, Fig. 8, bottom) the partially reduced catalyst exhibited a bulk-diffusion limited re-oxidation rate which coincides with an increased production of

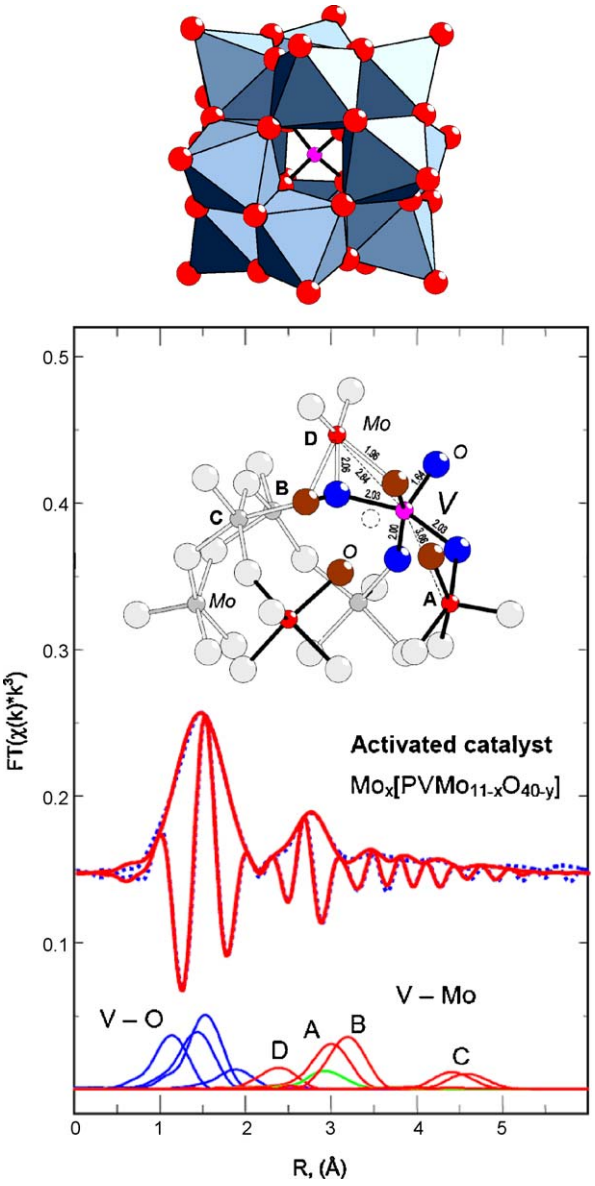

Fig. 7. Experimental (dotted) and theoretical FT($\chi(k)k^3$) of the V K edge spectra of activated $H_4[PVMo_{11}O_{40}]\cdot 13\ H_2O$ (denoted as $Mo_x[PVMo_{11-x}O_{40}]$) and single-scattering shells in the local structure around the V center in the Keggin ion. The inset shows a schematic representation of the local structure around the V center in the lacunary Keggin ion of $Mo_x[PVMo_{11-x}O_{40}]$. The regular Keggin ion structure of HPOM is also depicted.

carbon dioxide and, hence, a reduced selectivity of the catalyst. The production of CO_2 decreased with the increasing re-oxidation of the catalyst and, after complete re-oxidation, the catalyst reached its original activity and selectivity. Both $H_3[PMo_{12}O_{40}]$ and $H_4[PVMo_{11}O_{40}]$ exhibited a very similar structural evolution during treatment in propene and under selective oxidation conditions. The resulting activated catalysts possess a low reducibility and improved selectivity compared to α-MoO_3. The superior catalytic performance of activated $H_4[PVMo_{11}O_{40}]$ should therefore be attributed to a facilitated formation of the active sites and a functional promoting effect of the additional V centers.

3.3. Correlation between average valence and catalytic selectivity of MoO_3 supported on SBA-15

The Mo K near-edge spectra and the Fourier transformed XAFS $\chi(k)$ function of MoO_3 supported on SBA-15 are similar to those of

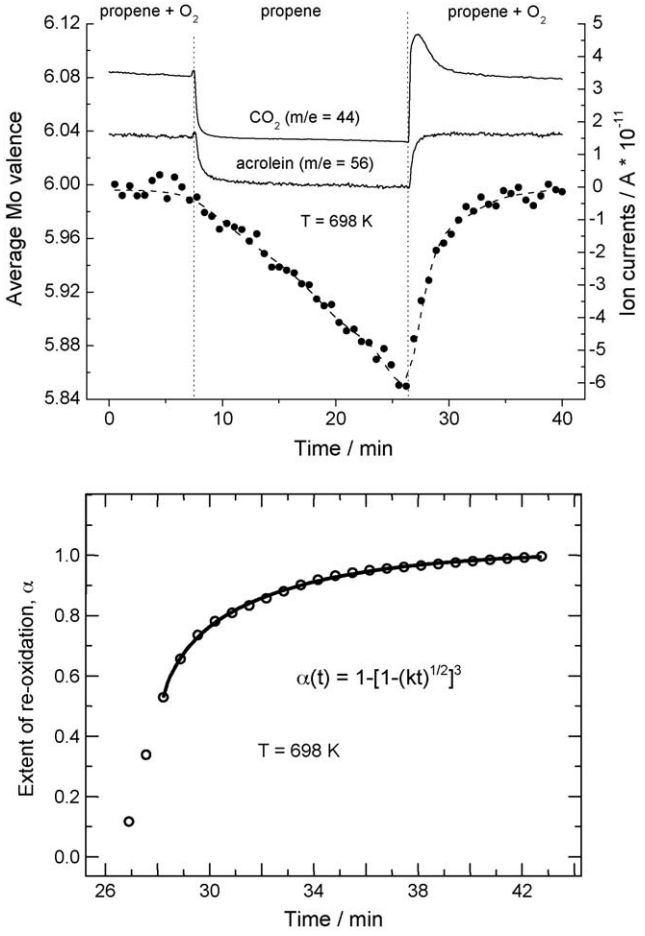

Fig. 8. Evolution of Mo average valence of activated $H_5[PV_2Mo_{10}O_{40}]\cdot 13H_2O$ during changing gas phase composition (propene to propene and oxygen) together with the corresponding evolution of acrolein and CO_2 in the gas phase at 698 K (top). Refinement of a solid-state kinetic model for three-dimensional solid-state diffusion ($\alpha(t) = 1 - [1 - (kt)^{1/2}]^3$) to the experimental extent of re-oxidation of activated $H_5[PV_2Mo_{10}O_{40}]\cdot 13H_2O$ at 698 K (bottom).

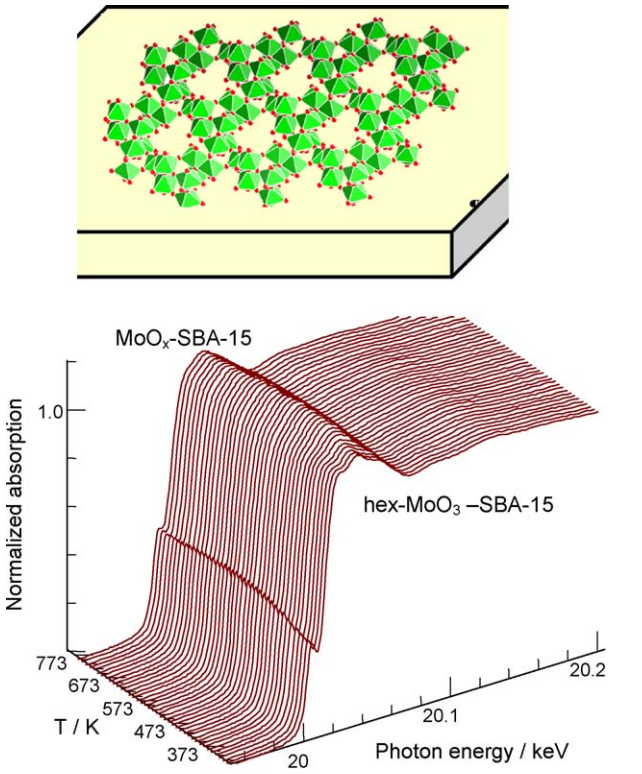

Fig. 9. Evolution of Mo K near-edge spectra (bottom) of hexagonal MoO_3 supported on SBA-15 (top) during temperature-programmed treatment in propene (300–773 K, 4 K/min, 1% propene in He).

hexagonal MoO_3 [18,28]. Nanostructured SiO_2 materials such as SBA-15 [32] constitute suitable support systems to permit in situ studies on the hexagonal modification of MoO_3. Analysis of the Mo K edge position yields an average valence of 6. Apparently, no isolated MoO_x species on SiO_2 were detected. A detailed analysis of the EXAFS function of MoO_3 supported on SBA-15 resulted in a predominantly two-dimensional hexagonal MoO_3 structure (denoted as hex-MoO_3-SBA-15).

Hex-MoO_3-SBA-15 exhibited a surprising stability compared to bulk hex-MoO_3 or α-MoO_3. Calcination of ammonium heptamolybdate in air results in a temporary formation of hexagonal MoO_3 which rapidly transforms to α-MoO_3 upon further heating. [33] Conversely, hex-MoO_3-SBA-15 is stable at 773 K in air. Similarly, the reduction behavior of hex-MoO_3-SBA-15 differs from that of bulk hexagonal MoO_3 and α-MoO_3. The evolution of Mo K near-edge spectra of hex-MoO_3-SBA-15 during temperature-programmed reduction in propene (300–773 K, 4 K/min, 1% propene in He) is depicted in Fig. 9. In contrast to the behavior of bulk hex-MoO_3 or α-MoO_3 during TPR in propene (Fig. 2), hex-MoO_3-SBA-15 is not fully reduced to MoO_2 during treatment in propene at 773 K. Apparently, the strong interaction between the hexagonal MoO_3 and SBA-15 support that inhibits the formation of α-MoO_3 under oxidative conditions also prevents the reduction to MoO_2 in propene. The very low reducibility and the formation of an activated species during treatment in propene is similar to the previously described behavior of $H_5[PV_2Mo_{10}O_{40}]$) under reaction conditions (Figs. 7 and 8) [31].

The low reducibility of hex-MoO_3 on SBA-15 and activated $H_5[PV_2Mo_{10}O_{40}]$) indicate that pronounced oxygen mobility in the bulk may not necessarily be required for good catalytic performance. Hence, the high oxygen mobility in α-MoO_3 is a byproduct of its bulk structure but no prerequisite for its catalytic activity. In order to further elucidate the stability and catalytic properties of hex-MoO_3-SBA-15 under changing reaction conditions, oxygen was added temporarily to the propene feed at 723 K. Prior to the addition of oxygen, hex-MoO_3-SBA-15 was treated in propene at 773 K for 15 min. Similar to the behavior of $H_5[PV_2Mo_{10}O_{40}]$) this resulted only in a slight reduction of the Mo oxide phase as can be seen from the decreased Mo K pre-edge peak (Fig. 10). Subsequently, oxygen was added to the propene feed at 723 K and switched off again after 20 min. During the isothermal re-oxidation phase (propene + O_2 on) and the re-reduction phase (only propene on) Mo K edge XANES spectra were collected with a time-resolution of 30 s. EXAFS analysis after the switching experiments indicated that the structure of the molybdenum oxide phase supported on SBA-15 still corresponded to that of hexagonal MoO_3.

The evolution of the XANES spectra and of the MS ion traces of CO_2, H_2O, and acrolein measured during addition of oxygen to the propene feed at 723 K are depicted in Fig. 10 (the jump in the m/e 56 signal at ~5 min was probably caused by a slight change in pressure and sensitivity of the MS). While the concentration of CO_2 in the gas phase exhibited a spiked increase, the concentration of acrolein increased more slowly. The evolution of the Mo K edge position during the oxidation and reduction treatment at 723 K is depicted in Fig. 11(top). Upon adding oxygen to the propene feed at 723 K, the Mo K edge shifted to higher energies indicative of an increasing average Mo valence (average Mo valence of 5.8 after

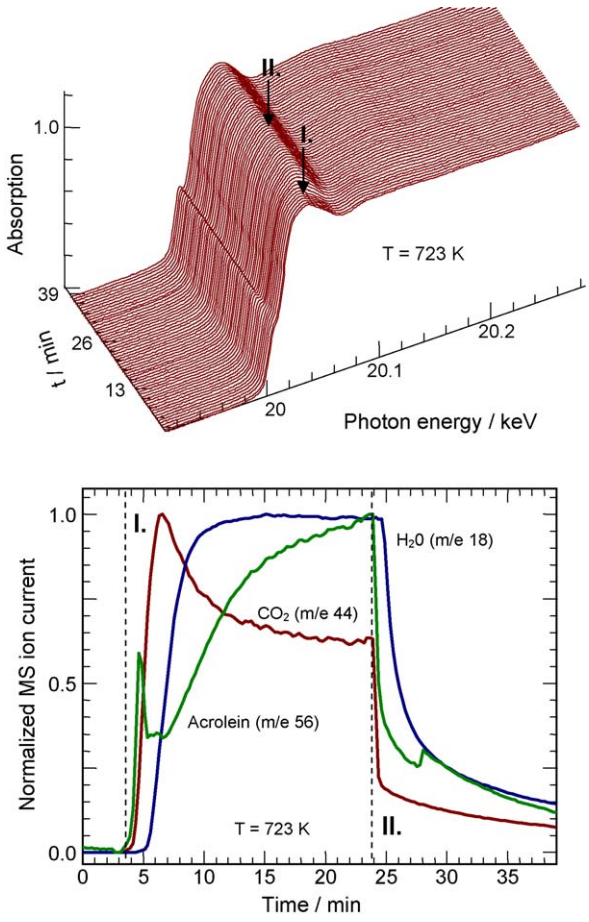

Fig. 10. Evolution of Mo K near-edge spectra during isothermal (T = 723 K) addition of oxygen (5% oxygen in He) during treatment of hex-MoO_3-SBA-15 in propene (1% propene in He) (I. - oxygen on; II. - oxygen off) (top). Evolution of normalized ion currents of H_2O (m/e 18), acrolein (m/e 56), and CO_2 (m/e 44) obtained by mass spectrometric analysis of the gas phase composition during isothermal addition of oxygen (A). Dashed lines indicate oxygen on (~3.5 min, I.) or oxygen off (~24 min, II.) (bottom).

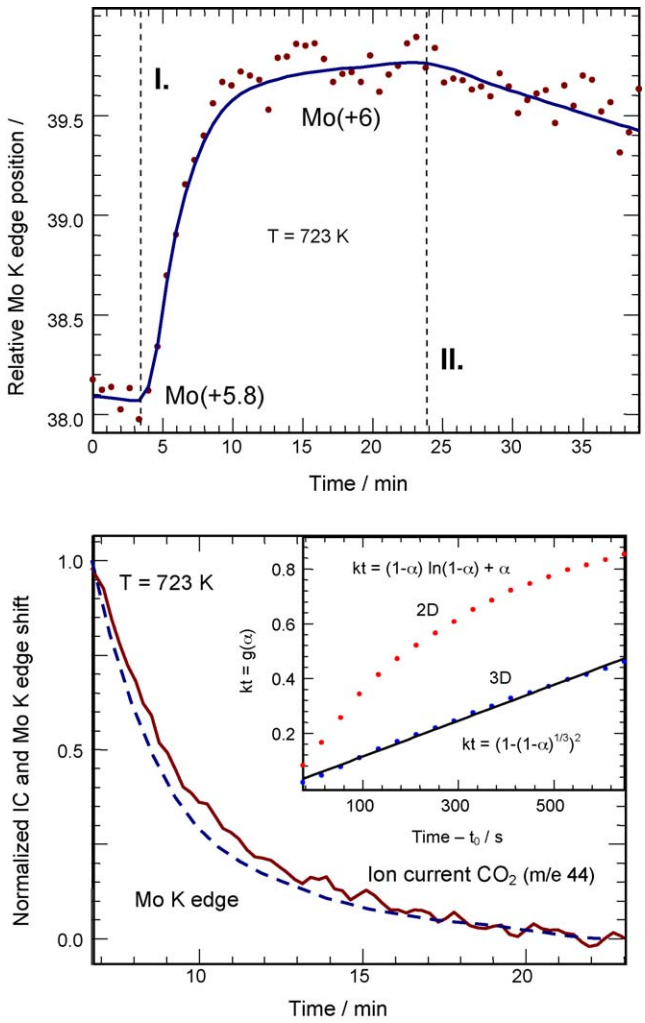

Fig. 11. Evolution of relative Mo K edge position during isothermal (T = 723 K) addition of oxygen (5% oxygen in He) during treatment of hex-MoO_3-SBA-15 in propene (1% propene in He) (Fig. 10) (top). The average Mo valence in the reduced state (~2 min) and the re-oxidized state (~20 min) is indicated. Dashed lines correspond to addition (~3.5 min, I.) or removal (~ 24 min, II.) of oxygen. Normalized ion current (IC) of CO_2 (m/e 44) together with normalized Mo K edge position during addition of oxygen (phase I. in Fig. 10) (bottom). The inset shows the integrated function $g(\alpha)$ of the extent of reduction α for a two-dimensional (2D) and three-dimensional (3D) diffusion solid-state kinetic model.

treatment in propene at 773 K and of ~6.0 after re-oxidation in propene and oxygen (~ 20 min in Fig. 11)). Fig. 11(bottom) correlates the re-oxidation rate of the Mo oxide phase in propene and oxygen with the decreasing CO_2 concentration in the gas phase (Fig. 10). Apparently, the increase in Mo average valence and the decrease in CO_2 formation proceed at about the same rate. The inset in Fig. 11(bottom) shows the integrated function $g(\alpha)$ [34] of the extent of oxidation α calculated for two solid-state kinetics models (i.e. two-dimensional diffusion or three-dimensional diffusion as rate-limiting step). The inverted and normalized Mo K edge shift depicted in Fig. 11(top) was taken as extent of oxidation α. During the first 3 min after adding oxygen to the propene feed the rate of re-oxidation of the Mo is mainly determined by transport of oxygen into the in situ cell. Here, surface or near-surface Mo centers are rapidly re-oxidized. After three minutes a solid-state kinetic model that assumes three-dimensional diffusion in the Mo oxide bulk to be the rate-limiting step was suited best to simulate the experimental α trace (i.e. Mo K edge shift, $g(\alpha)$ linear with time) (Fig. 11(bottom)). Moreover, Fig. 11 indicates a correlation between the time-dependent change of the average Mo valence and the selectivity of the MoO_x-SBA-15 phase under selective oxidation reaction conditions. This behavior is similar to that of activated polyoxomolybdates (i.e. $H_5[PV_2Mo_{10}O_{40}]$) during alternating treatment in propene and propene and oxygen as described above. While a more reduced MoO_x-SBA-15 catalyst exhibited a decreased selectivity, the selectivity increased with increasing average Mo valence during re-oxidation of MoO_x-SBA-15 in propene and oxygen.

3.4. Correlation between solid-state kinetics, electronic structure, and catalytic selectivity

The correlation between re-oxidation kinetics and catalytic performance corroborates the assumption, that the selectivity of the catalyst is governed by its electronic structure. The latter in turn appears to be determined by the defect structure of the underlying bulk. On the one hand, lattice oxygen in α-MoO_3 is readily available to the reactant propene and, thus, α-MoO_3 is rapidly and completely reduced to MoO_2. On the other hand, complete re-oxidation to MoO_3 is hindered by formation of characteristic "$Mo_{18}O_{52}$" type defects and their oxidation kinetics. Thus, α-MoO_{3-x} exhibits a reduced average valence under reaction conditions and an inferior catalytic selectivity. Conversely, hexagonal MoO_3 stabilized on a SiO_2 support or activated HPOM catalyst studied, exhibit a much lower reducibility. Apparently,

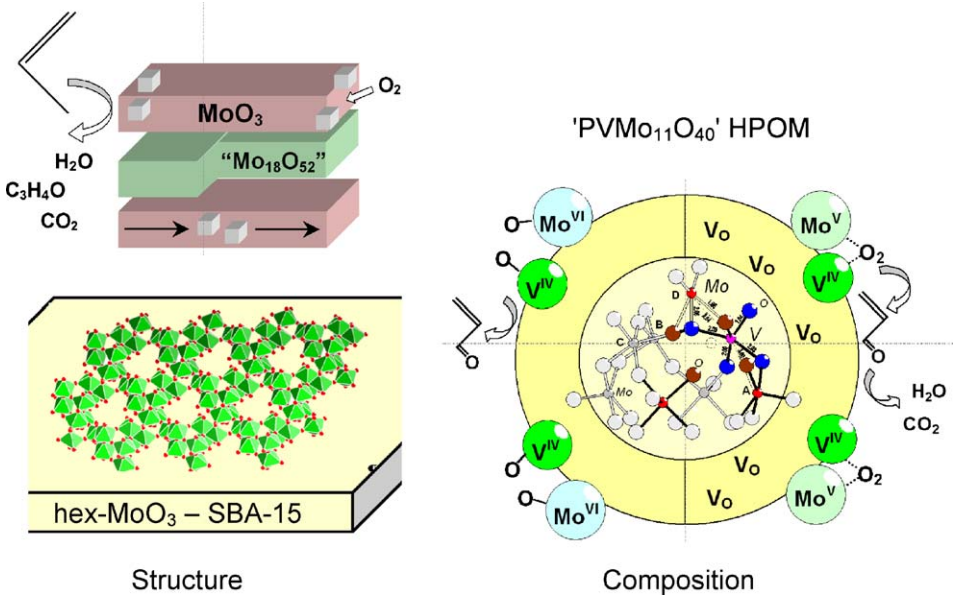

Fig. 12. Schematic representation of various model catalysts under propene oxidation reaction conditions; (left) influence of structural motif on reducibility, redox solid-state kinetics, average valence under reaction conditions and, hence, improved selectivity; (right) influence of additional V centers as functional promoters in the "active site" of HPOM catalysts.

their defect structure and re-oxidation kinetics under reaction conditions permits complete re-oxidation to an average Mo valence of 6. Under these conditions a superior selectivity compared to α-MoO_3 is observed. It may be concluded, that on a material that exhibits high reducibility, hindered re-oxidation, and a prolonged lifetime of partially reduced Mo metal sites, total oxidation of propene will dominate. On the other hand, catalytic oxidation of propene proceeding on a fully oxidized Mo site at the surface of the catalyst yields an improved selectivity towards partial oxidation products.

Some tentative suggestions regarding the effect of structural and compositional complexity of molybdenum oxide based catalysts on their performance are summarized in Fig. 12. Onset of selective oxidation activity coincides with the availability of lattice oxygen from the catalyst bulk/surface. With oxygen becoming sufficiently mobile in bulk of the catalyst, the average valence and, hence, the density of partially reduced Mo sites, is determined by the interplay of the reduction and re-oxidation kinetics of the molybdenum oxide. Fast and complete re-oxidation kinetics of a "suitable" structure guarantees a high average valence which appears to be correlated with high selectivity. Moreover, "suitable" structures for highly selective oxidation catalysts may be envisaged without additional metal centers (Fig. 12, left). Compositional complexity is no prerequisite for a superior catalyst. Of course, "suitable" structures can be stabilized by additional metal centers, which may overall be their primary role. Furthermore, within the same "suitable" structure, additional metal centers may indeed facilitate formation of active sites and functionally promote the catalytic behavior of this site (Fig. 12, right).

4. Concluding remarks

The examples presented here demonstrate the potential of time-resolved XAS investigations. A suitable time resolution extends the applicability of XAS from in situ studies in heterogeneous catalysis to investigations under dynamic conditions. XAS experiments under stationary conditions reveal the structure of the working catalyst. However, correlations between the structure of the catalyst and its catalytic properties can more readily be elucidated from monitoring the structural response of the catalyst to (rapidly or even periodically) changing reaction conditions. Certainly, solid-state kinetics can also be obtained from complementary methods such as TG/DTA, TPR, or TPRS, whereas complementary in situ techniques (e.g. XRD, Raman, IR, UV–vis) can provide structural and/or valence information under reaction conditions. However, the capability of XAS combined with a time-resolution in the second range makes it a very powerful tool for studies on solid-state kinetics in heterogeneous catalysis to reveal *quantitative phase composition and average valence* together with the *evolution of the local structure* of a system under rapidly changing conditions.

Acknowledgements

The Hamburger Synchrotron Radiation Laboratory, HASYLAB, and the European Synchrotron Radiation Facility, ESRF, are acknowledged for providing beamtime for the various investigations described. Financial support by the Deutsche Forschungsgemeinschaft (DFG) is gratefully acknowledged.

References

[1] B. Grzybowska-Swierkosz, Top. Catal. 11–12 (2000) 23–42.
[2] R.K. Grasselli, Catal. Today 49 (1999) 141–153.
[3] J. Haber, E. Lalik, Catal. Today 33 (1997) 119–137.
[4] M.M. Bettahar, G. Costentin, L. Savary, J.C. Lavalley, Appl. Catal. A 145 (1996) 1–48.
[5] P. Mars, D.W. van Krevelen, Chem. Ing. Sci. 3 (41) (1954).
[6] L.D. Krenzke, G.W. Keulks, J. Catal. 61 (1980) 316–325.
[7] W. Ueda, Y. Moro-Oka, T. Ikawa, J. Catal. 70 (1981) 409–417.
[8] B. Grzybowska, J. Haber, J. Janas, J. Catal. 49 (150) (1977).
[9] K. Brückmann, R. Grabowski, J. Haber, A. Mazurkiewicz, J. Sloczynski, T. Wiltowski, J. Catal. 104 (71) (1987).
[10] B.M. Weckhuysen (Ed.), In-situ Spectroscopy of Catalysts, American Scientific Publishers, Los Angeles, USA, 2004;
J.F. Haw (Ed.), In-Situ Spectroscopy in Heterogeneous Catalysis, Wiley-VCH, New York, USA, 2002;
B. Gates, H. Knoezinger, Advances in Catalysis, vol. 51, Elsevier, 2007;
B. Gates, H. Knoezinger, Advances in Catalysis, vol. 52, Elsevier, 2009 and references therein.
[11] B.L. Kniep, T. Ressler, A. Rabis, F. Girgsdies, M. Baenitz, F. Steglich, R. Schlögl, Angewandte Chemie Int Ed. 43 (2004) 112–115.
[12] M.M. Lin, Appl. Catal. A: Gen. 207 (2001) 1–16.
[13] T. Okuhara, N. Mizuno, M. Misono, Adv. Catal. 41 (2001) 443–673.
[14] T. Ressler, R.E. Jentoft, J. Wienold, T. Neisius, J. Catal. 210 (2002) 67–83.

[15] T. Ressler, R.E. Jentoft, J. Wienold, M.M. Günter, O. Timpe, J. Phys. Chem. B 104 (2000) 6360–6370.
[16] S. Berndt, D. Herein, F. Zemlin, E. Beckmann, G. Weinberg, J. Schütze, G. Mestl, R. Schlögl, Ber. Bunsenges. Phys. Chem. 102 (1998) 763.
[17] G.A. Tsigdinos, Top. Curr. Chem. 76 (1987) 1–64.
[18] Z. Huang, T. Vitoya, D. Deng, H. Modrow, W. Bensch, T. Ressler, J. Mater. Sci. 43 (1) (2008) 244–253.
[19] T. Ressler, J. Synch. Rad. 5 (1998) 118–122.
[20] J.J. Rehr, C.H. Booth, F. Bridges, S.I. Zabinsky, Phys. Rev. B 49 (1994) 12347–12350.
[21] T. Ressler, S.L. Brock, J. Wong, S.L. Suib, J. Phys. Chem. B 103 (1999) 6407–6420.
[22] P.A. Batist, C.J. Kapteijns, B.C. Lippens, G.C.A. Schuit, J. Catal. 7 (33) (1967).
[23] P.L. Gai-Boyes, Catal. Rev. Sci. Eng. 34 (1) (1992).
[24] M. Maciejewski, A. Baiker, A. Reller, Solid State Ionics 43 (203) (1990).
[25] L.E. Firment, A. Ferretti, Surf. Sci. 129 (155) (1983).
[26] T. Ressler, J. Wienold, R.E. Jentoft, O. Timpe, T. Neisius, Solid State Commun. 119 (2001) 169–174.
[27] T. Ressler, J. Wienold, R.E. Jentoft, F. Girgsdies, Eur. J. Inorg. Chem. 2 (2003) 301–312.
[28] T. Ressler, A. Walter, Z.-D. Huang, W. Bensch, J. Catal. 254 (2008) 170–179.
[29] J. Wienold, O. Timpe, T. Ressler, Chem. A Eur. J. 9 (2003) 6007–6017.
[30] T. Ressler, O. Timpe, F. Girgsdies, J. Wienold, T. Neisius, J. Catal. 231 (2005) 279–291.
[31] T. Ressler, O. Timpe, J. Catal. 247 (2007) 231–237.
[32] D.Y. Zhao, J.L. Feng, Q.S. Huo, N. Melosh, G.H. Fredrickson, B.F. Chmelka, G.D. Stucky, Science 279 (1998) 548.
[33] J. Wienold, R.E. Jentoft, T. Ressler, Eur. J. Inorg. Chem. 6 (2003) 1058–1071.
[34] C.H. Bamford (Ed.), Comprehensive Chemical Kinetics, vol. 2, Elsevier, 1968.